07.3

InAs/GaSb superlattices for infrared photodetectors

© A.K. Bakarov, M.A. Sukhanov, A.S. Jaroshevich, I.D. Loshkarev, K.S. Zhuravlev

Rzhanov Institute of Semiconductor Physics, Siberian Branch of Russian Academy of Sciences, Novosibirsk, Russia
E-mail: bakarov@isp.nsc.ru

Received May 17, 2024
Revised June 27, 2024
Accepted June 28, 2024

Focal plane array infrared photodetectors are highly demanded in various fields, including environmental protection, medicine and military applications. This paper presents the results of growing InAs/GaSb superlattice structures using molecular beam epitaxy on GaSb substrates for the mid— and longwave infrared photodetectors. Conditions for growing GaSb buffer layers and superlattices with In−Sb interfacial layer are defined. It is shown that a low arsenic concentration in the buffer layer has little effect on the structural quality of superlattices, while the buffer thickness has a more significant impact. The selected growth conditions allowed for high reproducibility of the superlattice period lengths. The measured superlattice layer thicknesses were close to those specified during the growth. The presence of the InSb interface resulted in good optical properties of the superlattices. High reproducibility of superlattices allowed us to control the longwave absorption edge by shifting it from 5.6 to 9 μm by merely adjusting the thicknesses of the InAs and GaSb layers.

Keywords: molecular beam epitaxy, type-II InAs/GaSb superlattices, infrared photodetectors.

DOI: 10.61011/0000000000

Photodetector arrays recording infrared (IR) radiation in the atmospheric transparency windows play an important role in various areas of human activity [1–3]. To make possible fabrication of highquality arrays and their largevolume application, it is important to provide them with good IR sensitivity and high manufacturability. It is desirable that the arrays be applicable in sufficiently lowcost photodetector devices not needing strong cooling.

Being used in creating photodetector arrays, a pair of A_3B_5 compounds, InAs and GaSb, possesses a number of unique properties: first, these substances have almost equal growthplane lattice parameters $a_{\mathrm{InAs}} = 6.0583$ Å and $a_{\mathrm{GaSb}} = 6.0959$ Å; second, in this case it is possible to create superlattices whose optical transition energies may be adjusted to the mid— (3−5 μm) and longwave (8−14 μm) IR ranges by varying thicknesses of the InAs and GaSb layers [4]. As compared to the cadmium−mercury−tellurium solid solutions, chemical bonds in gallium antimonide and indium arsenide are stronger, which makes the material more stable. In addition, production cost of the InAs/GaSb superlattices is lower, and GaSb substrates are relatively inexpensive and commercially available [5]. Relative to IR photodetectors based on intersubband transitions in AlGaAs/GaAs quantum wells (QWIP), photodetectors based on InAs/GaSb superlattices have a higher absorption coefficient and exhibit high quantum efficiency for photons incident normal to the surface [1].

In the periodic InAs/GaSb structure, the InAs conduction band bottom lies below the GaSb valence band top, electrons and holes are localized in different layers, and a type-II superlattice (commonly designated as T2SL) is formed. In [6], T2SL absorption was calculated by the kp method for superlattices with different thicknesses of InAs and GaSb layers at different temperatures; the calculations agree well with experimental data.

In this work, T2SLs consisting of alternating InAs/GaSb layers with the thicknesses (in monolayers) of 8 ML/13 ML (T2SL1) and 13.5 ML/7 ML (T2SL2), 100 repetitions per each superlattice, were grown by molecular beam epitaxy (MBE). The structures were grown at a Riber Compact-21T setup on GaSb(100) substrates doped with tellurium with the electron concentration of $5 \cdot 10^{17}$ cm^{-3}. Fluxes of the fifth group materials (As and Sb) were generated by valved cells. The cracking zone temperature in the cells was 900°C; therefore, fluxes of dimers As_2 and Sb_2 were generated. Growth rates of third group materials were calibrated with respect to oscillations of the specularly reflected fast electron diffracted beams and were 0.2 ML/s for InAs and 0.4 ML/s for GaSb. In the T2SL1 and T2SL2 samples, GaSb buffer layers 250 and 500 nm thick, respectively, were grown on the substrate. In the process of growing the buffer layers, the substrate temperature was 500°C, while that in growing superlattices was 400°C. The In−Sb bonds were formed at each superlattice interface, which is optimal for achieving high optical characteristics of such superlattices [7]. For this purpose, after the growth of each InAs superlattice layer was completed, first the arsenic flux was shut off, and the indium flux was shut off in 1 s after this; due to this, an indium enriched surface superstructure (4×2) was formed. This surface was exposed to the antimony flux for 3 s, after which the GaSb layer was grown. Upon the growth of the GaSb layer, the surface was kept in the antimony flux for 3 s; after the antimony flux was shut off, the indium shutter was open for 1 s, and then the InAs growth began.

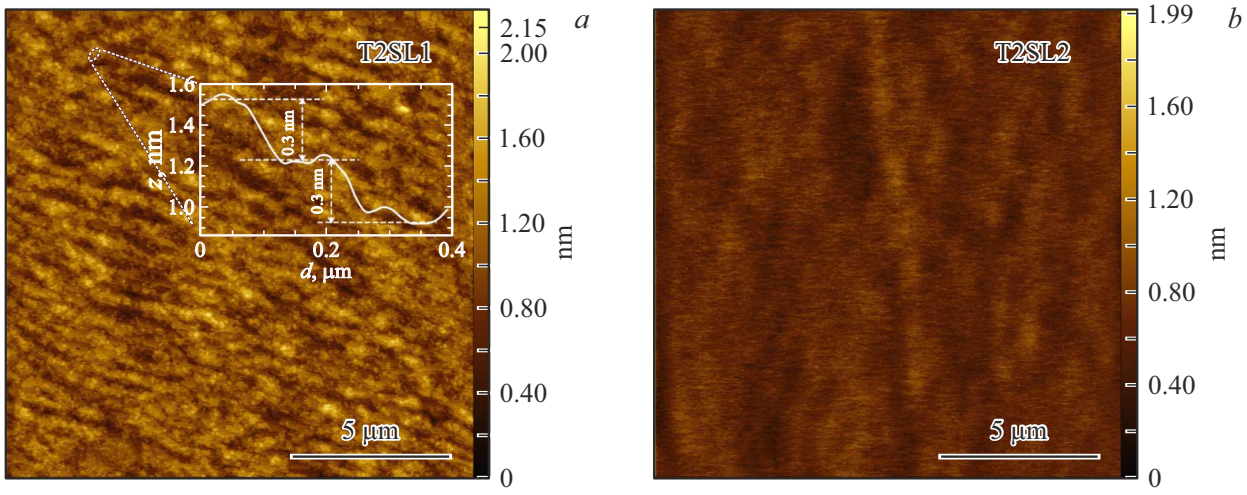

Figure 1. AFM images of the T2SL1 (*a*) and T2SL2 (*b*) surfaces. Steps approximately 100 nm wide and 0.3 nm high are visible, which matches with the monolayer height of the terrace.

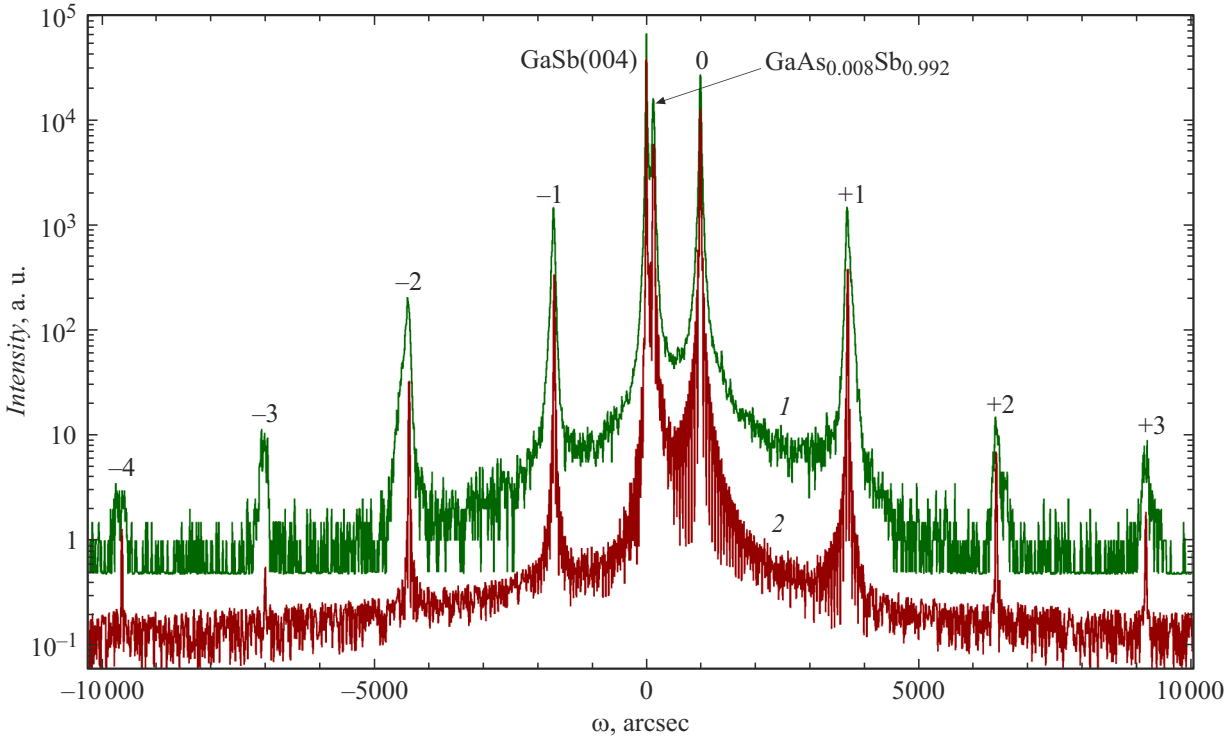

Figure 2. Experimental (*1*) and calculated (*2*) diffraction reflection curves obtained in the geometry of symmetric reflection (004) for the T2SL2 sample.

To characterize the surface morphology of the grown superlattices, measurements with an atomic force microscope (AFM) were performed in the areas $15 \times 15\,\mu$m in size (Fig. 1). The T2SL1 surface is rough, with hills about 0.6 nm high and 300 nm wide. Analysis of the height profile showed the stepped character of the surface (see the inset in Fig. 1). The T2SL2 surface is smoother. Statistical analysis of AFM images gave the rootmeansquare surface roughness of 0.24 nm for T2SL1 and 0.13 nm for T2SL2.

Structural perfection of the samples was analyzed by X-ray diffraction using a double crystal X-ray diffractometer with a Ge(004) monochromator crystal and Cu$K_{\alpha 1}$ ($\lambda = 1.54056$ Å) radiation. Fig. 2 demonstrates the experimental and calculated T2SL2 diffraction reflection curves (DRC) obtained in the geometry of reflection symmetric about the (004) node. DRCs exhibit the GaSb substrate peak, GaAsSb buffer layer peak, and satellite peaks from the periodic structure. The zero satellite position

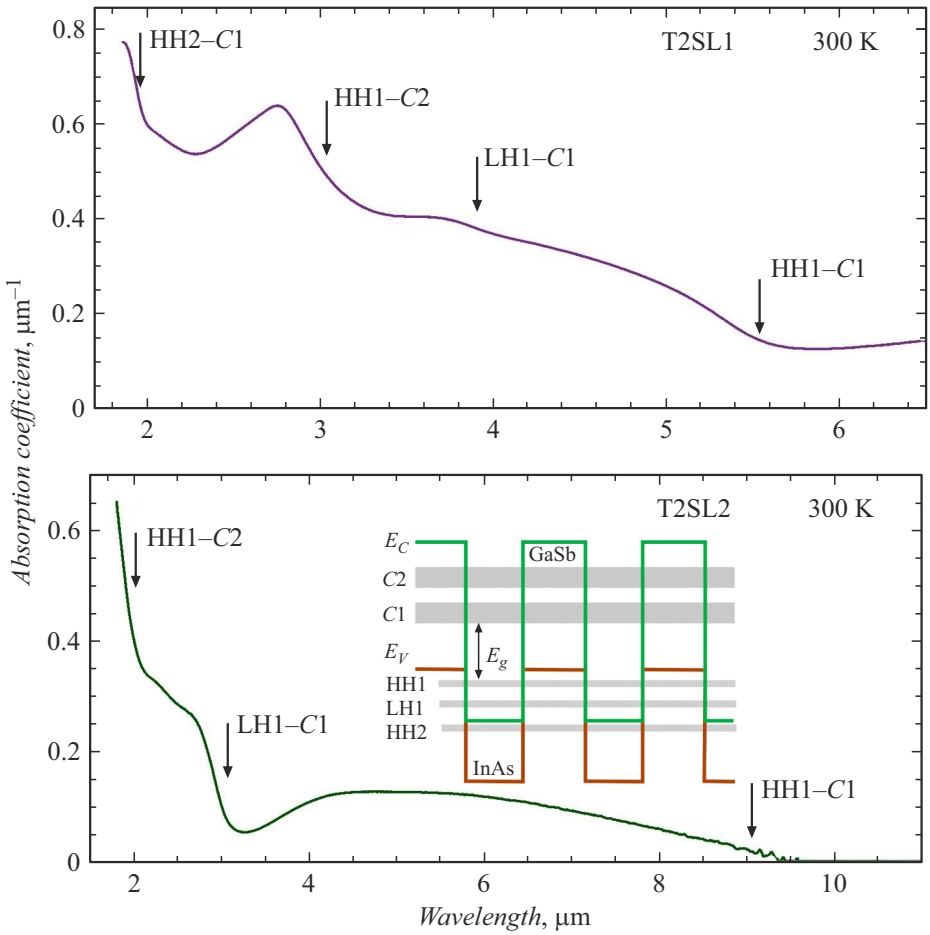

Figure 3. Superlattice absorption spectra. The inset schematically represents the edges of the InAs and GaSb conduction and valence bands, as well as minibands of electrons ($C1$ and $C2$), heavy holes (HH1 and HH2) and light holes (LH1) emerging in the superlattice. Arrows indicate the transition points as per [13].

corresponds to the average elemental composition of the superlattice.

We associate the emergence of a peak near the GaSb(004) substrate peak in the T2SL2 DRC with adding arsenic to the buffer layer and formation of the $GaAs_xSb_{1-x}$ solid solution. The peak shift by +130 arcsec corresponds to $x \approx 0.8\%$. The background arsenic in the MBE setup has probably remained after growth of A_3 arsenides; this was previously observed in [8,9]. The bufferlayer and substrate peaks in the T2SL1 sample DRC coincide with each other. Mismatches of the average lattice parameters of T2SL1 and T2SL2 with the substrate, which were determined based on the zero satellite shift from the substrate peak, equaled $\Delta a/a = 0.129$ and 0.267%, respectively, which is because of high InAs content in T2SL2. Full widths at half height of the T2SL1 and T2SL2 zero satellites are 200 and 30 arcsec, respectively, which means that T2SL2 structural perfection is higher. This is consistent with the AFM data. The thicker GaAsSb buffer layer has probably a smoother surface than the thin GaSb buffer layer, despite the roughness inherent of solid solution [10], and remains smoother during the entire structure growth. Angular distance between the satellites depends on the superlattice period thickness. In the studied structures, satellites of up to the fourth order are observed, which confirms high quality and strict periodicity of superlattices. Note that the T2SL2 layer thicknesses 14.7 ML/7.9 ML, specified in the DRC simulation are close to those specified for the superlattice growth (13.5 ML/7 ML).

IR absorption spectra were obtained using vacuum Fouriertransform spectrometer Bruker Vertex 80v with computeraided attachment A510/Q-T designed for measuring transmission and reflectance. The angle of radiation incidence on the sample was 11°. Light scattered by the sample was collected in the solid angle of ±5°. As a source of IR radiation, a globar and KBr-based light beam splitter were used. Vacuum conditions were such as to prevent the effect of atmospheric impacts on the spectra measured in the range of $1-25\,\mu$m. In the experiments there were measured reflection and transmission spectra of the T2SL1 and T2SL2 superlattices, as well as of the GaSb substrate. To determine the substrate absorption α and reflection R coefficients based on the measured substrate reflectance R_m and transmittance T_m, first R were

obtained by numerically solving the righthand equality of the transcendental expression taken from [11]:

$$\exp(-2\alpha d) = \frac{(1-R-A_m)^2}{(1-R-RA_m)^2} = \frac{R_m - R}{R(1-2R+RR_m)}, \quad (1)$$

where A_m is the absorbability, d is the substrate thickness. Substrate absorption coefficient α was calculated from calculated R. Using the obtained values of the substrate α and R and measured superlattice transmittance, the superlattice absorption coefficient was calculated via the formula from [12]:

$$T_{mS} = \frac{(1-R)^2 \exp(-\alpha d)\exp(-\alpha_S d_S)}{1-R^2\exp(-2\alpha d)\exp(-2\alpha_S d_S)}. \quad (2)$$

Here T_{mS} is the measured superlattice transmittance, α_S is the superlattice absorption coefficient, d_S is the superlattice thickness. The superlattice absorption coefficients are presented in Fig. 3.

The longwave edge of the T2SL1 absorption band is $\sim 5.6\,\mu$m, while that for T2SL2 is $\sim 9\,\mu$m. The obtained absorption spectra are close in both the absorption curve amplitude and shape to the spectra of similar InAs/GaSb superlattices obtained in [6,13,14]. The spectrum shape is determined by the oscillator strengths which depend on the superlattice layer thicknesses. The inset to Fig. 3 schematically shows minibands emerging in the superlattice energy spectrum.

Thus, the article demonstrates the results of growing short period strained type-II InAs/GaSb superlattices on GaSb substrates and examining their structural and optical properties. The study has shown that the selected conditions for growing the buffer and superlattices and forming heterointerfaces with the In–Sb bonds between the superlattice layers allow for obtaining superlattices with high period repeatability and good optical characteristics. The surface morphology and structural perfection of the samples get improved with increasing buffer layer thickness. The measured superlattice layer thicknesses were close to those specified for growing the superlattices. The edge of the superlattice absorption spectrum was controlled by shifting it towards the red range due to varying thicknesses of their layers: from ~ 5.6 to $\sim 9\,\mu$m. The superlattice optical characteristics are close to those of the worldbest samples.

Funding

The study was accomplished under the State Assignment for ISP SB RAS (project № FWGW-2022-0005).

Conflict of interests

The authors declare that they have no conflict of interests.

References

[1] A. Rogalski, P. Martyniuk, M. Kopytko, Appl. Phys. Rev., **4** (3), 31304 (2017). DOI: 10.1063/1.4999077
[2] D. Ramos, M. Delmas, L. Höglund, R. Ivanov, L. Žurauskaité, D. Evans, D. Rihtnesberg, L. Bendrot, S. Smuk, A. Smuk, S. Becanovic, S. Almqvist, P. Tinghag, S. Fattala, E. Costard, P.E. Hellström, Appl. Phys. Lett., **123** (18), 181102 (2023). DOI: 10.1063/5.0176652
[3] D. Kwan, M. Kesaria, E.A. Anyebe, D. Huffaker, Infrared Phys. Technol., **116**, 103756 (2021). DOI: 10.1016/j.infrared.2021.103756
[4] D.O. Alshahrani, M. Kesaria, E.A. Anyebe, V. Srivastava, D.L. Huffaker, Adv. Photon. Res., **3** (2), 2100094 (2021). DOI: 10.1002/adpr.202100094
[5] M. Walther, R. Rehm, J. Schmitz, J. Niemasz, F. Rutz, A. Wörl, L. Kirste, R. Scheibner, J. Wendler, J. Ziegler, Proc. SPIE, **7945**, 79451N (2011). DOI: 10.1117/12.875159
[6] Y. Livneh, P.C. Klipstein, O. Klin, N. Snapi, S. Grossman, A. Glozman, E. Weiss, Phys. Rev. B, **86** (23), 235311 (2012). DOI: 10.1103/physrevb.86.235311
[7] Y. Zhang, W. Ma, Y. Cao, J. Huang, Y. Wei, K. Cui, J. Shao, IEEE J. Quantum Electron., **47** (12), 1475 (2011). DOI: 10.1109/jqe.2011.2168947
[8] A. Jasik, J. Kubacka-Traczyk, K. Regiński, I. Sankowska, R. Jakieła, A. Wawro, J. Kaniewski, J. Appl. Phys., **110** (7), 73509 (2011). DOI: 10.1063/1.3642995
[9] A. Jasik, I. Sankowska, K. Regiński, E. Machowska-Podsiadło, A. Wawro, M. Wzorek, R. Kruszka, R. Jakieła, J. Kubacka-Traczyk, M. Motyka, J. Kaniewski, in: *Crystal growth: theory, mechanisms and morphology*, ed. by J.P. Isaac, N.A. Manusco (Nova Science Publ., Inc., 2012), ch. 9, p. 293–327.
[10] B.J. Spencer, P.W. Voorhees, J. Tersoff, Phys. Rev. B, **64** (23), 235318 (2001). DOI: 10.1103/physrevb.64.235318
[11] D.C. Look, J.H. Leach, J. Vac. Sci. Technol. B, **34** (4), 04J105 (2016). DOI: 10.1116/1.4954211
[12] G. Ariyawansa, E. Steenbergen, L.J. Bissell, J.M. Duran, J.E. Scheihing, M.T. Eismann, Proc. SPIE, **9070**, 90701J (2014). DOI: 10.1117/12.2057506
[13] P.-F. Qiao, S. Mou, S.L. Chuang, Opt. Express, **20** (3), 2319 (2012). DOI: 10.1364/oe.20.002319
[14] H. Katayama, T. Takekawa, M. Kimata, H. Inada, Y. Iguchi, Infrared Phys. Technol., **70**, 53 (2015). DOI: 10.1016/j.infrared.2014.10.014

Translated by EgoTranslating